ORIGINAL PAPER

Effect of Eu_2O_3 Nanoparticles Addition on Structural and Superconducting Properties of BSCCO

**Amir Zelati · Ahmad Amirabadizadeh ·
Ahmad Kompany · Hadi Salamati · Jeff Sonier**

Abstract To study the effects of Eu_2O_3 nanoparticles addition to BSCCO superconducting system, four bulk polycrystalline samples with general formula of $Bi_{1.6}Pb_{0.4}Sr_2Ca_2Cu_3O_y + x Eu_2O_3$ (where $x = 0.0, 0.3, 0.5, 1.0$ wt%) were prepared by chemical sol–gel method. X-ray diffraction, SEM, and TEM were used for structural characterization of the samples. DC electrical resistivity, critical current, and AC magnetic susceptibility were measured. XRD analysis showed that both (Bi,Pb)-2223 and Bi-2212 phases coexist in the samples having orthorhombic crystal structure. DC electrical resistivity, J_c, and AC magnetic susceptibility measurements reveal that adding Eu nanoparticles to BSCCO improves superconducting properties of this system and enhances its critical current density. The enhancement of the J_c may be caused by improvement of the grain connectivity with Eu nanoparticle additions.

Keywords Bi-2223 · AC magnetic susceptibility · DC electrical resistivity · Critical current density · XRD · SEM

A. Zelati (✉) · A. Amirabadizadeh
Department of Physics, University of Birjand, Birjand, Iran
e-mail: a_zelati@yahoo.com

A. Kompany
Department of Physics, Ferdowsi University of Mashhad, Mashhad, Iran

H. Salamati
Faculty of Physics, Isfahan University of Technology, Isfahan, Iran

J. Sonier
Depatment of Physics, Simon Fraser University, Burnaby, BC, Canada

1 Introduction

Since the discovery of Bi-based superconducting systems, a great amount of work concerning preparation, superconducting properties, and the structure of these compounds has been done [1–3]. The BSCCO system, mainly contains three phases in the general formula $Bi_2Sr_2Ca_{n-}Cu_nO_{2n+4+y}$ where $n = 1, 2$ and 3 refers to the number of CuO_2 layers which yields 10, 95 and 110 K superconducting phases, respectively [4]. The Bi-2201, Bi-2212 and Bi-2223 phases have single, double and triple layers of CuO_2 in the subunit cell, respectively. It is believed that in BSCCO system more CuO_2 planes is associated with higher value of T_c ($R = 0$) [5, 6]. The superconducting properties of BSCCO system can be controlled by addition or substitution of elements. The enhancement or destruction of the superconducting properties depends on the characteristics of the dopant in the crystal structure. Pb is the most important substituting element that influences the microstructure, phase composition, and the related superconducting properties of BSCCO system. The presence of Pb in the initial mixture favors the reaction kinetics of Bi-2223 phase [7, 8]. Pb addition results in the creation of a superconducting solid solution $Bi_{2-x}Pb_xSr_2Ca_2Cu_3O_d$ by partial substitution of bismuth and the optimal Pb content (x) lies between 0.3 and 0.4, so $x = 0.4$ was selected for preparing the samples in this report [9, 10]. Despite many efforts to obtain Bi-2223 single phase, preparation of BSCCO systems normally leads to the coexistence of (Bi,Pb)-2223 and Bi-2212 phases in the samples.

In the application of the BSCCO superconductors, higher critical current density (J_c) plays a more significant role than the other factors. However, the major limitations of the BSCCO superconductor applications are the intergrain weak links and weak flux pinning capability, which lead to weak critical current density in bulk samples. There have been remarkable improvements in enhancing transport properties

of this high-T_c superconductor since when BSCCO superconductor was discovered. The superconducting properties of BSCCO system can be enhanced by addition or substitution of elements with different ionic radius and different bonding character. As an example, to obtain more applicable BSCCO sample one can add or substitute metallic elements to the BSCCO system to improve the connectivity between grains leading to higher J_c [11]. Several researchers [12–16] have investigated the effect of substitution or addition of rare earth oxides and some other oxides on the superconducting and structural properties of BSCCO system. The works of most of these researches are related to addition or substitution of micro-oxide powders to BSCCO systems.

With nanotechnology developments, a wide range of nanostructure materials have been synthesized. In the nano-size range, the particles have a high proportion of atoms located at their surface as compared to bulk materials, giving rise to unique physical and chemical properties that are very different from their bulk counterparts [17]. In recent years, studying the effect of addition or substitution of nanoparticles to BSCCO system has been of much interest (see, for example, Refs. [18–21] and the references therein). When nanoparticles are added to the BSCCO system, due to the tiny size of nanoparticles, they settle easier and much more among the grains of these ceramic superconductors than the micro size dopants. If adequate amount of nanoparticles with metallic character is added to the BSCCO, the intergrain connectivity will possibly improve.

In this study, we added Eu_2O_3 nanoparticles to the BSCCO system in order to improve the connectivity between grains. We generally expect that addition of a small amount of Eu nanoparticles in BSCCO system would enhance connectivity between the grains due to metallic character of Eu, or would make possible pinning centers between grain boundaries. The general formula for preparing the samples of this research was $Bi_{1.6}Pb_{0.4}Sr_2Ca_2Cu_3O_y + xEu_2O_3$ and $x = 0.0, 0.3, 0.5, 1.0$ wt%. The BSCCO sample was prepared by chemical sol–gel method [22–25] and Eu_2O_3 nanopowder by combustion method. XRD, SEM, TEM, EDX, and selected area electron diffraction (SAED) were used for morphological and structural characterization of the prepared samples. DC resistivity, J_c, and AC magnetic susceptibility measurements were performed to study the superconducting properties of the samples and to achieve the optimal amount of Eu nanoparticle addition to the BSCCO system.

2 Experimental

2.1 Sample Preparation

The samples were prepared according to the general formula $Bi_{1.6}Pb_{0.4}Sr_2Ca_2Cu_3O_y + xEu_2O_3$ and $x = 0.0, 0.3, 0.5, 1.0$ wt% in three steps as follows:

Step 1 BSCCO sample with chemical composition $Bi_{1.6}Pb_{0.4}Sr_2Ca_2Cu_3O_y$ was prepared by chemical sol–gel method, using the powders of $Bi(NO_3)_2 \cdot 5H_2O$, $Pb(NO_3)_2$, $Sr(NO_3)_2$, $Ca(NO_3)_2 \cdot 4H_2O$ and $Cu(NO_3)_2 \cdot 3H_2O$, as the starting materials. EDTA with chemical composition $N_2H_{10}O_{16}$ was used as the complexing agent with the molar ratio EDTA:cation $= 1$, ethylene glycol (EG) with chemical composition $C_2H_4(OH)_2$ as the binding agent of complexes with the molar ratio EG:cation $= 3$ and urea as the fuel with the molar ratio urea:cation $= 0.7$. Distilled water and nitric acid were used as a solvent. Bismuth nitrate was poured in appropriate volume of distilled water (400 mL for 40 gr final production) at temperature 40 °C. A certain amount of nitric acid was added to the mixture to make a bismuth solution. Then the other nitrates were added to this solution. After stirring the mixture, a transparent blue solution with pH $= 1$ was obtained, which we named the material solution. After that, a certain amount of EG was solved in appropriate volume of distilled water (400 mL for 50 gr final production) at temperature 40 °C and then EDTA was added to this solution which resulted in the formation of precipitation. In order to annihilate the precipitation, NH_3OH was added to the liquid mixture so that a transparent solution with pH $= 6$ was obtained (the main solution). The material solution was poured into the main solution drop by drop at temperature 60 °C until the starting the formation of the precipitation. At this time, the process of adding the material solution to the main solution was stopped to eliminate the precipitation via NH_3OH. This process was repeated until all the material solution was added to the main solution and obtaining the gel with pH $= 4$. The next performance was adding urea, as the fuel to the prepared gel. Then, the urea added gel was dried on a hot plate with gradually increasing temperature from 60 to 200 °C, which took 3 days to complete the process of drying. At the end of this time a rather weak combustion occurred and a gray colored powder was produced. The powder was ground and calcined at 850 °C for 7 h in air. After calcination a black powder was obtained. The prepared powder was then ground and divided in four segments.

Step 2 Eu_2O_3 nanoparticles were prepared by combustion method using europium (III) nitrate pantahydrate with chemical composition $Eu(NO_3) \cdot 5H_2O$ as starting material. Distilled water was used as the solvent and glycine with chemical formula $C_2H_5NO_2$ as the fuel of the reaction. Europium (III) nitrate pantahydrate was solved in adequate amount of distilled water. After obtaining aqueous solution of cation, Eu^{3+}, glycine as the fuel for combustion was added to the solution. The liquid mixture was placed inside the preheated (300 °C) oven for one hour. Combustion took place inside the oven and russet smoke of the NO_2 gas came out. The resultant product was a voluminous, foamy

white powder. Later, XRD pattern and TEM images confirmed the cubic structure and the nano-size of the prepared Eu_2O_3 powder.

Step 3 Eu_2O_3 nanopowder, in this step, was added to each of the segments (1, 2, 3 and 4) prepared in the first step with 0.0, 0.3, 0.5 and 1.0 wt%, respectively. Each sample was ground and calcined at 850 °C for 7 h in air. The calcined powders were ground again and pressed under 450 MPa pressure to form pellets 11 mm in diameter and 3.5 mm thick. The prepared pellets were finally sintered at 860 °C for 24 h in air. A sample with $x = 0.0$ in general chemical formula, $Bi_{1.6}Pb_{0.4}Sr_2Ca_2Cu_3O_y + xEu_2O_3$, was labeled as sample A and the other samples labeled as B ($x = 0.3$), C ($x = 0.5$), and D ($x = 1.0$).

2.2 Sample Characterization

XRD, SEM, TEM, EDX and SAED were used for the structural studies of the samples. DC resistivity, J_c, and AC magnetic susceptibility measurements were carried on to study the superconducting properties of the samples. The X-ray powder diffraction pattern for each sample was obtained using CuKα (1.54 Å) radiation in the range $2\theta = 20$–$65°$ by a Rigaku R-Axis Diffractometer. Phase purity and the lattice parameters were obtained from these patterns. SEM and TEM imaging were used to examine the surface morphology and grain structure of the samples and EDX was applied for the elemental analysis of the samples. SEM images were taken by using a Strata Dual beam 235 field emission scanning electron microscope. TEM images, EDX spectra and SAED patterns were obtained by using a TecnaiG2 scanning transmission electron microscope (STEM). The R–T behavior of the samples from 30 K to room temperature was investigated in order to determine the superconducting transition temperature. The electrical resistance measurements and J_c determination were performed using the standard four-probe method. The magnetic susceptibility measurements were carried out employing a Quantum Design SQUID magnetometer MPMS-XL7 that works between 1.8 and 400 K with a 7 Tesla superconducting magnet. Diamagnetic corrections were applied for the sample holder and the core diamagnetism of the samples.

3 Results and Discussion

3.1 X-Ray Diffraction and Microstructure Studies

XRD patterns of $Bi_{1.6}Pb_{0.4}Sr_2Ca_2Cu_3O_y + xEu_2O_3$ ($x = 0.0$, 0.3, 0.5, and 1.0 wt%) samples indicated that all the samples consisted of two phases, Bi-2212 and Bi-2223 (Fig. 1).

The XRD patterns revealed that all the samples consisted of (2212) and (2223) phases, with (2223) phase being the dominant one. To estimate the volume fraction of the present phases, we used the corresponding Bi-2212 and Bi-2223 peaks, and the following formulas [18]:

$$\text{Bi-(2223)}\% = \frac{\sum I(2223)}{\sum I(2223) + I(2212)} \times 100$$

$$\text{Bi-(2212)}\% = \frac{\sum I(2212)}{\sum I(2223) + I(2212)} \times 100$$

where $I(2223)$ and $I(2212)$ are the intensities of the (hkl) XRD peaks for Bi-2223 and Bi-2212, respectively. The calculated relative portions of each phase of the samples are listed in Table 1. As seen in the table, samples with $x = 0.0$, 0.3, 0.5 and 1.0 contained 76, 80, 84 and 70 % of the 2223 phase, respectively. The percent amounts of the 2223 and 2212 phases as a function of x evaluated from the XRD patterns of $Bi_{1.6}Pb_{0.4}Sr_2Ca_2Cu_3O_y + xEu_2O_3$ ($x = 0.0$, 0.3, 0.5 and 1.0) samples are given in Fig. 2. It is seen that the volume fraction of the Bi-2223 phase increases with increasing Eu nanoparticle concentration up to $x = 0.5$, while a decrease in the volume fraction of the Bi-2223 phase is observed for sample D ($x = 1$ wt%).

The crystal system of Eu-free sample was found to be orthorhombic with the lattice parameters $a = 5.315$ Å, $b = 5.419$ Å and $c = 37.298$ Å. Almost, the same lattice parameters were obtained for the Eu nanoparticles-added samples. The results are given in Table 1. There is no distortion in the crystal system of the Eu-added Bi-2223, which shows that Eu particles do not participate in the crystal structure of the Bi-2223. We believe that the added nanoparticles are sited between the superconducting grains. The role of such impurity nanoparticles can be either as the pinning centers to fix vortices or enhancing connectivity between grains, which may lead to higher J_c [11].

Figure 3 displays the surface SEM images of the Eu nanoparticles-free and -added samples. It is observed that the microstructures of all samples exhibit a common feature of plate-like grains and are randomly distributed. We believe that white particles sited between the grains are Eu nanoparticles, which is obvious in the micrographs of Eu-added samples. These particles can enhance the connectivity among the grains and they can increase the pinning centers to fix the vortices. SEM results corroborate well with XRD results. In addition to the intergranular distribution of the nanoparticles, the presence of the nanoparticles can be observed in the other parts of microstructure of Eu-added samples. Grains size of the sample D decreases comparing to the other samples, which may cause to a decrease in superconducting properties of this sample.

TEM images and EDX spectra from the powders of the Eu nanoparticles-added samples are presented in Fig. 4.
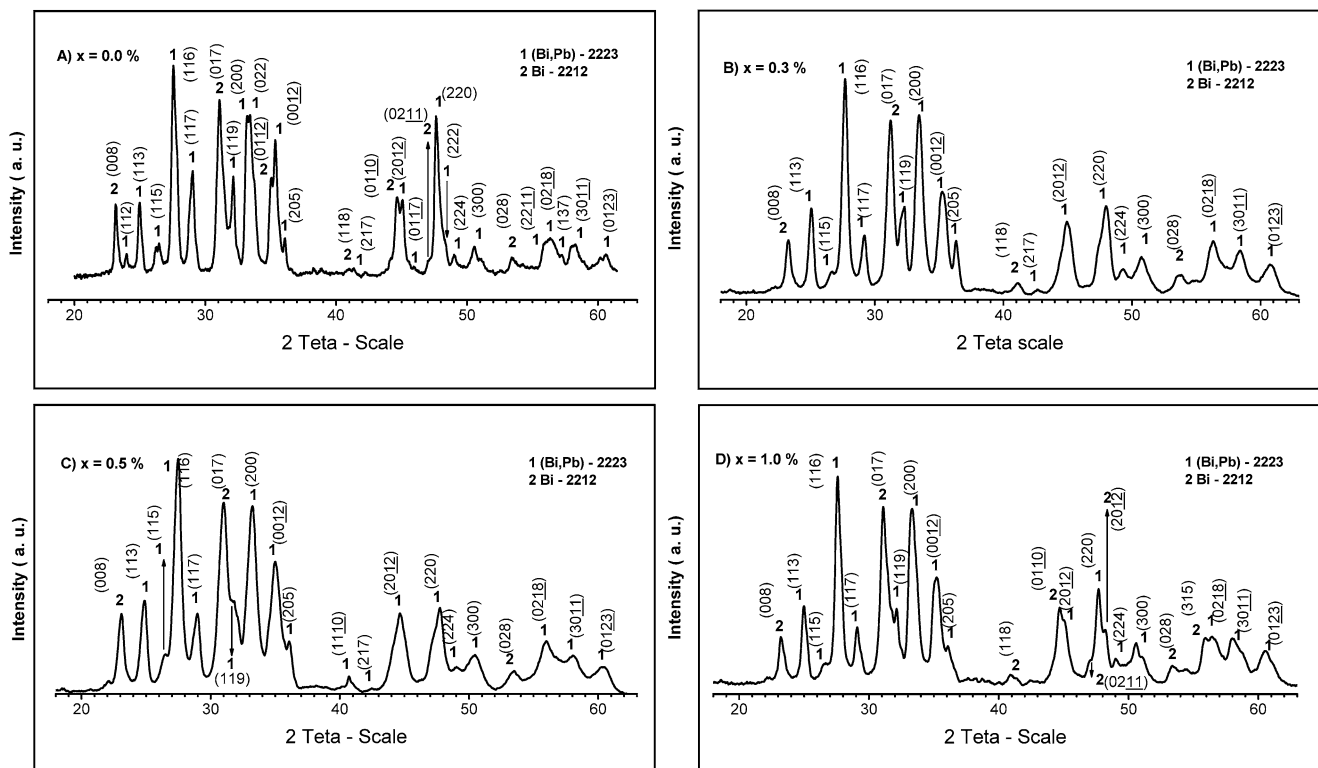
Fig. 1 XRD patterns of $Bi_{1.6}Pb_{0.4}Sr_2Ca_2Cu_3Oy + xEu_2O_3$ samples: (**A**) $x = 0.0$, (**B**) $x = 0.3$, (**C**) $x = 0.5$ and (**D**) $x = 1.0$ wt%. Peaks of (Bi,Pb)-2223 and Bi-2212 phases are indexed 1 and 2, respectively

Table 1 The lattice parameters and percentage volume fraction of Bi-2223 and Bi-2212 phases in $Bi_{1.6}Pb_{0.4}Sr_2Ca_2Cu_3Oy + xEu_2O_3$ ($x = 0.0$–1.0) samples

Sample	Orthorhombic unit cell (Bi-2223 phase)			Volume fraction of phase formed (%)	
	A (Å)	b (Å)	c (Å)	Bi-2223 phase	Bi-2212 phase
A	5.315	5.419	37.289	76	24
B	5.320	5.425	37.297	80	20
C	5.319	5.417	37.293	84	16
D	5.308	5.411	37.269	70	30

TEM images show that the grains are micro sized, which is essential in BSCCO system as a ceramic superconductor. Furthermore, the presence of the Eu nanoparticles can be clearly observed close to the grain boundaries. EDX was utilized to confirm the chemical composition of the synthesized samples, especially for the Eu-added samples. As shown in Fig. 4, Ca, O, Cu, Eu, Pb, Bi, and Sr peaks are presented in Eu-added samples. The morphology and size distribution of the Eu_2O_3 nanoparticles prepared for this work are shown in Fig. 5. The TEM image of the sample confirms the nano-size of the particles in the range of 5–80 nm. The histogram shows that the average particle size of Eu_2O_3 sample is about 33 nm.

SAED patterns of Eu-free sample taken along the [100] and [001] zone-axis directions of orthorhombic crystal, re-

spectively, are shown in Fig. 6(a)–(b). Since for the other samples there is no significant variation in the SAED patterns, only SAED patterns for Eu-free sample are shown. The ratio of the lattice parameter b/a based on these patterns is about 1.02, which is close to the value obtained by the XRD results [26, 27]. Indexing of the two important planes has been elucidated in diffraction pattern.

The theoretical density of BPSCCO system is about 6.3 g/cm^3 obtained from the lattice parameters [28]. The density of pellets in this work was determined as 5.48, 5.23, 5.11, and 4. 92 g/cm^3 for $x = 0.0$ to $x = 1.0$, respectively, measured by water displacement Archimedes method. The bulk densities obtained by Archimedes technique is in the range of 78 to 87 % of the theoretical values. This result is

in accordance with the porous structure of ceramic superconductors.

3.2 Superconducting Properties Measurements

As shown in Fig. 7, DC electrical resistance (R–T) reveals that the resistivity of the presented samples decreases linearly with temperature in the normal state. All the samples displayed a metallic character above onset temperature, which is defined as the temperature where R–T plot deviates from linearity [10]. Derivatives of the R–T curves were calculated to obtain the zero onset transition to the super-

Fig. 2 Volume fraction of Bi-(2223) and Bi-(2212) phases determined from XRD patterns

conducting state. The plots of the samples have a shoulder, which we believe to be due to the coexistence of Bi-2223 and Bi-2212 phases. The onset critical temperature ($T_{c,\text{onset}}$) and the zero resistivity critical temperature ($T_{c,R=0}$) of the samples are tabulated in Table 2. As seen in the table, $T_{c,\text{onset}}$ of the samples A, B, and C is 109.5 K and for sample D is 107 K. It is seen that $T_{c,R=0}$ shifts to higher temperatures with increasing Eu nanoparticle concentration up to $x = 0.5$ and the transition temperature width (ΔT_c) decreases, implying an enhancement in the intergrain connectivity [22, 23]. However for the sample D ($x = 1.0$), $T_{c,R=0}$ shifts to higher temperature comparing to Eu-free sample but since in sample D, $T_{c,\text{onset}}$ is lower than sample A, at this stage we cannot conclude that for this sample the improvement or destruction has occurred in the intergrain connectivity. The variation of T_c with Eu content, x, is given in Fig. 8.

A parabolic relationship holds between the superconducting transition temperature and the hole concentration. The hole concentration is calculated using the relation given below [29]:

$$p = 0.16 - [(1 - T_c / T_c^{\text{max}})/82.6]^{1/2}$$

where p indicates hole concentration and T_c^{max} is taken as 110 K for the Bi-2223 system. Previous calculations for the un-substituted Bi-2223 had shown that the values of p are
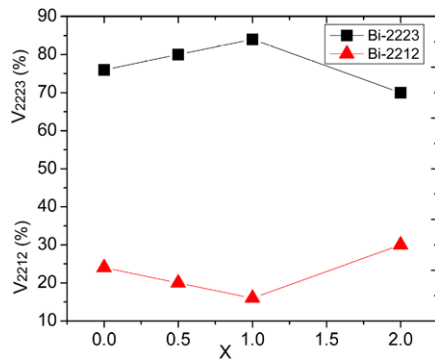

Fig. 3 SEM surface micrographs of $Bi_{1.6}Pb_{0.4}Sr_2Ca_2Cu_3Oy + xEu_2O_3$ samples, (**A**) $x = 0.5$, (**B**) $x = 0.5$, (**C**) $x = 1$ and (**D**) $x = 2$ wt%
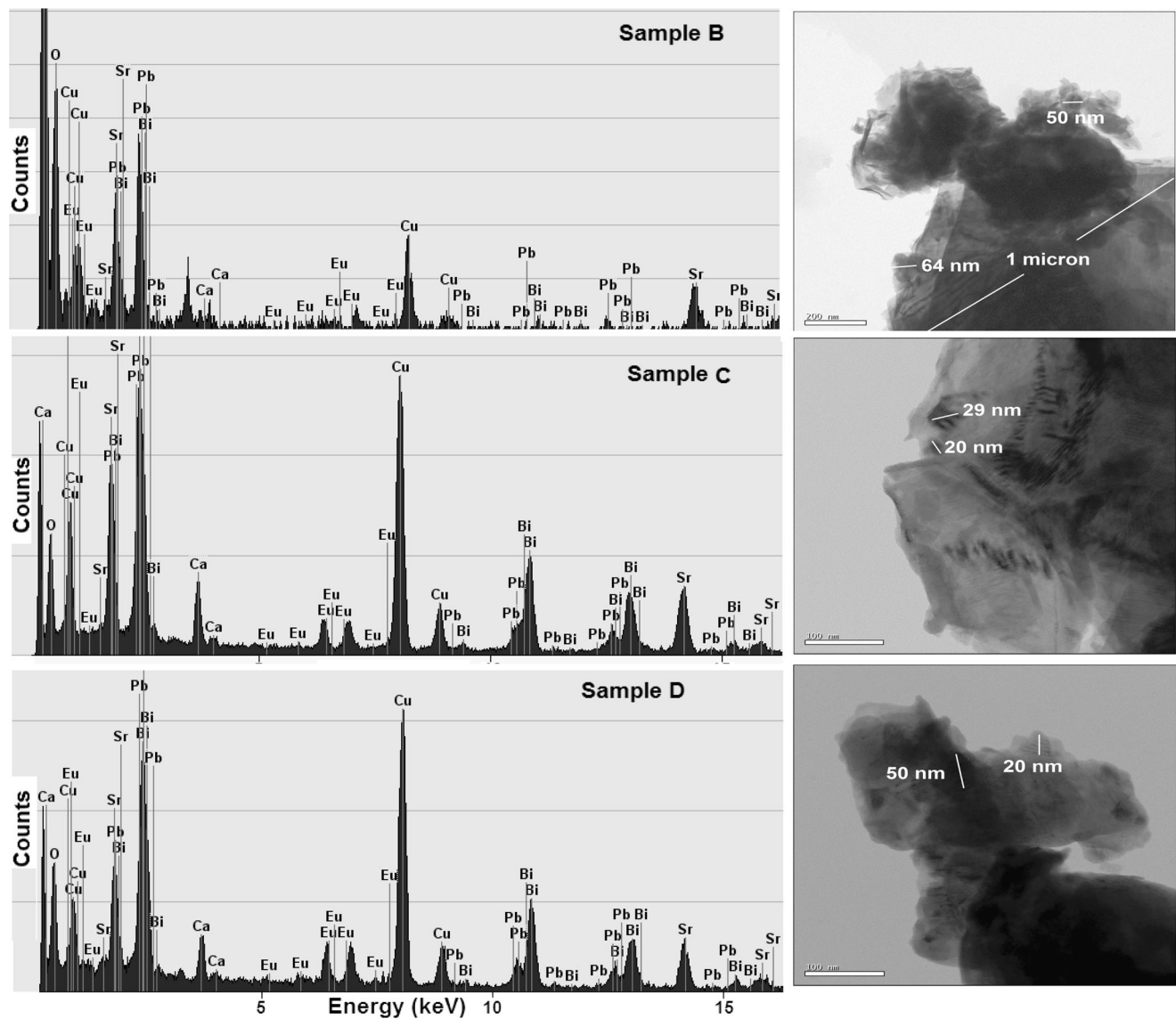
Fig. 4 TEM images and EDX spectra of the powders $Bi_{1.6}Pb_{0.4}Sr_2Ca_2Cu_3Oy + xEu_2O_3$ samples: (**B**) $x = 0.3$, (**C**) $x = 0.5$, and (**D**) $x = 1.0$

Table 2 The critical temperatures $T_{c,R=0}$ (K), $T_{c,onset}$ (K), ΔT_c (K) and mass density of $Bi_{1.6}Pb_{0.4}Sr_2Ca_2Cu_3O_y + xEu_2O_3$ samples

Sample	Eu (x)	$T_{c,onset}$ (K)	$T_{c,R=0}$ (K)	ΔT_c (K)	Mass density (g/cm^3)	J_c (A/cm^2)
A	0.0	109.5	79	30.5	5.48	15.90
B	0.3	109.5	81	28.5	5.23	19.87
C	0.5	109.5	83	26.5	5.11	27.34
D	1.0	107	80	27	4.92	10.33

in the range of 0.116 to 0.160 [29]. Figure 9 shows the critical temperature versus hole concentration plot. Hole carrier concentration varies from 0.1016 for Eu-free sample to 0.1055 for sample C ($x = 0.5$). The hole concentration increases in the samples with increasing Eu nanoparticle concentration up to $x = 0.5$, which may be the effect of

improvement in the intergrain connectivity of the samples. While for sample D with $x = 1.0$ the hole concentration starts to decrease to lower amounts, which can be caused by the destruction in the intergrain connectivity of this sample.

The critical current density of the samples was measured at temperature of 77 K in zero magnetic field as shown in

graphs of current density versus voltage in Fig. 10. J_c values of the samples are given in Table 2. According to the results, an enhancement in the critical current density of the Eu nanoparticle-added samples is observed, which is proportional to the concentration of the Eu in the samples B and C ($x = 0.3$ and 0.5), but not for sample D. This improvement in J_c may be attributed to the enhancement in the intergrain connectivity.

AC susceptibility measurement ($\chi' + i\chi''$) is widely used as a nondestructive method for determination and charac-
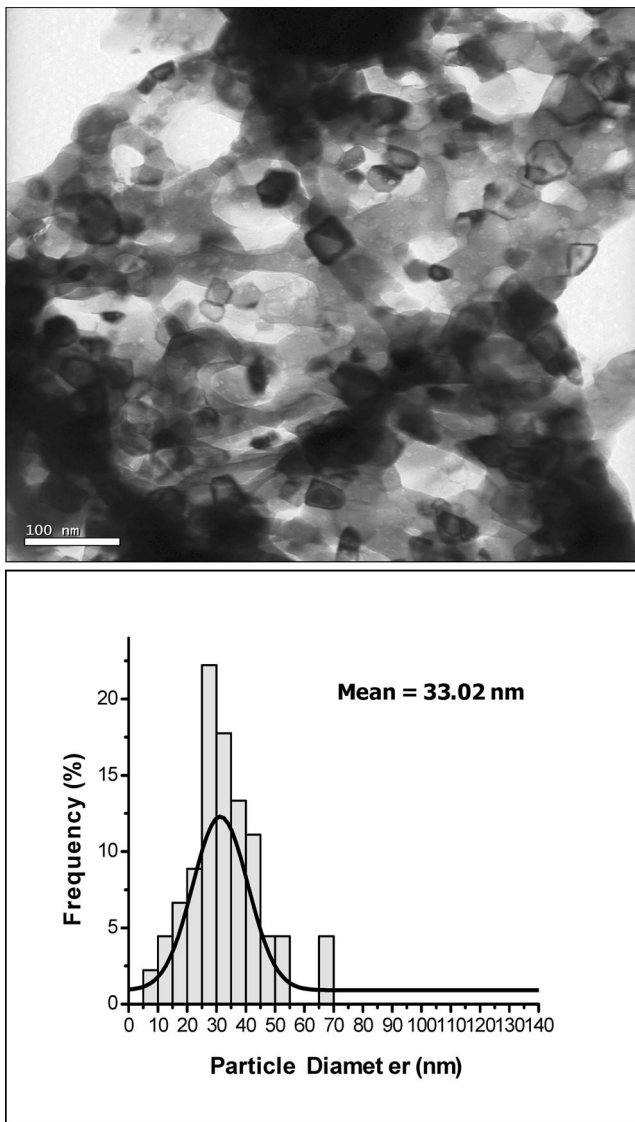
Fig. 5 TEM image and histogram of Eu$_2$O$_3$ nanoparticles
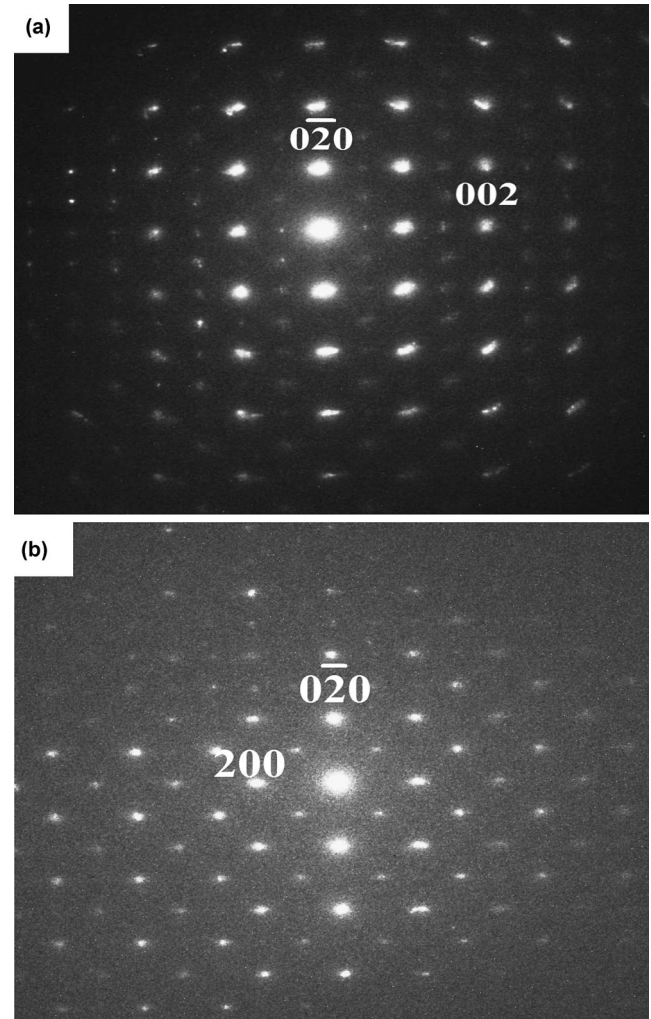
Fig. 6 Electron diffraction patterns of the orthorhombic Bi$_{1.6}$Pb$_{0.4}$Sr$_2$Ca$_2$Cu$_3$Oy (**a**) [100], (**b**) [001]
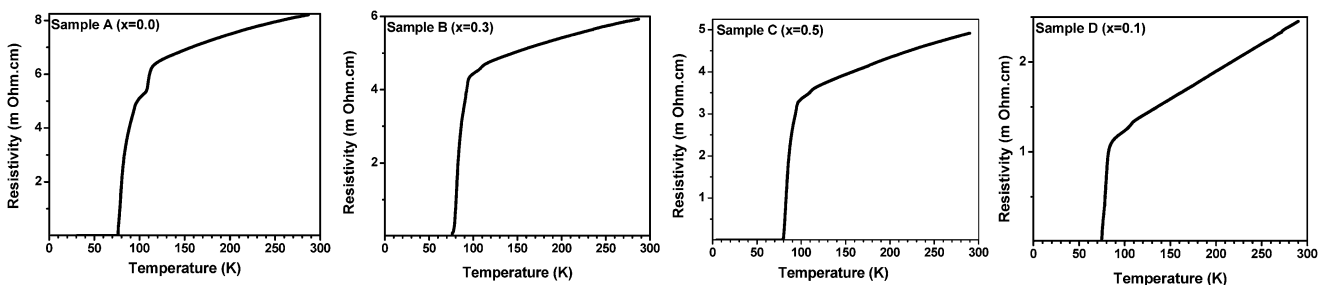
Fig. 7 Temperature dependences of the electrical resistivity for Bi$_{1.6}$Pb$_{0.4}$Sr$_2$Ca$_2$Cu$_3$O$y + x$Eu$_2$O$_3$ samples: (**A**) $x = 0.0$, (**B**) $x = 0.3$, (**C**) $x = 0.5$, and (**D**) $x = 1$

terization of the intra- and inter-grain features of the high-temperature superconductors. The in-phase component of fundamental susceptibility, χ', shows two significant drops

as the temperature is decreased below T_c for granular superconductors. The sharp drop near T_c corresponds only to the intrinsic properties of the grains. Another drop at low tem-
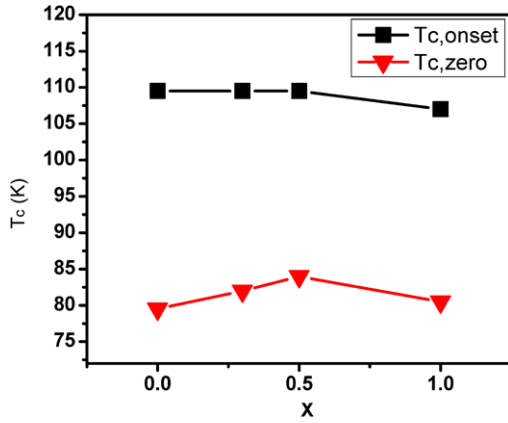

Fig. 8 Variation of critical temperature of $Bi_{1.6}Pb_{0.4}Sr_2Ca_2Cu_3Oy + xEu_2O_3$ ($x = 0.0$–1.0) samples
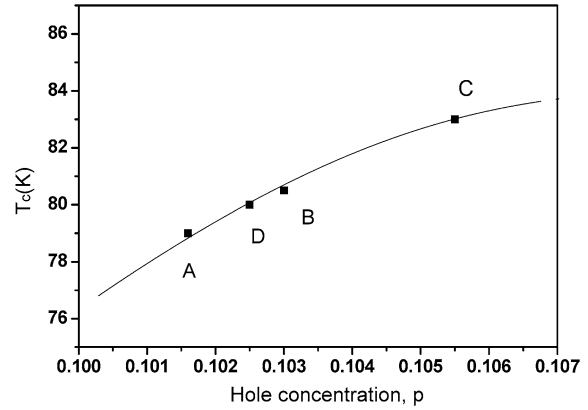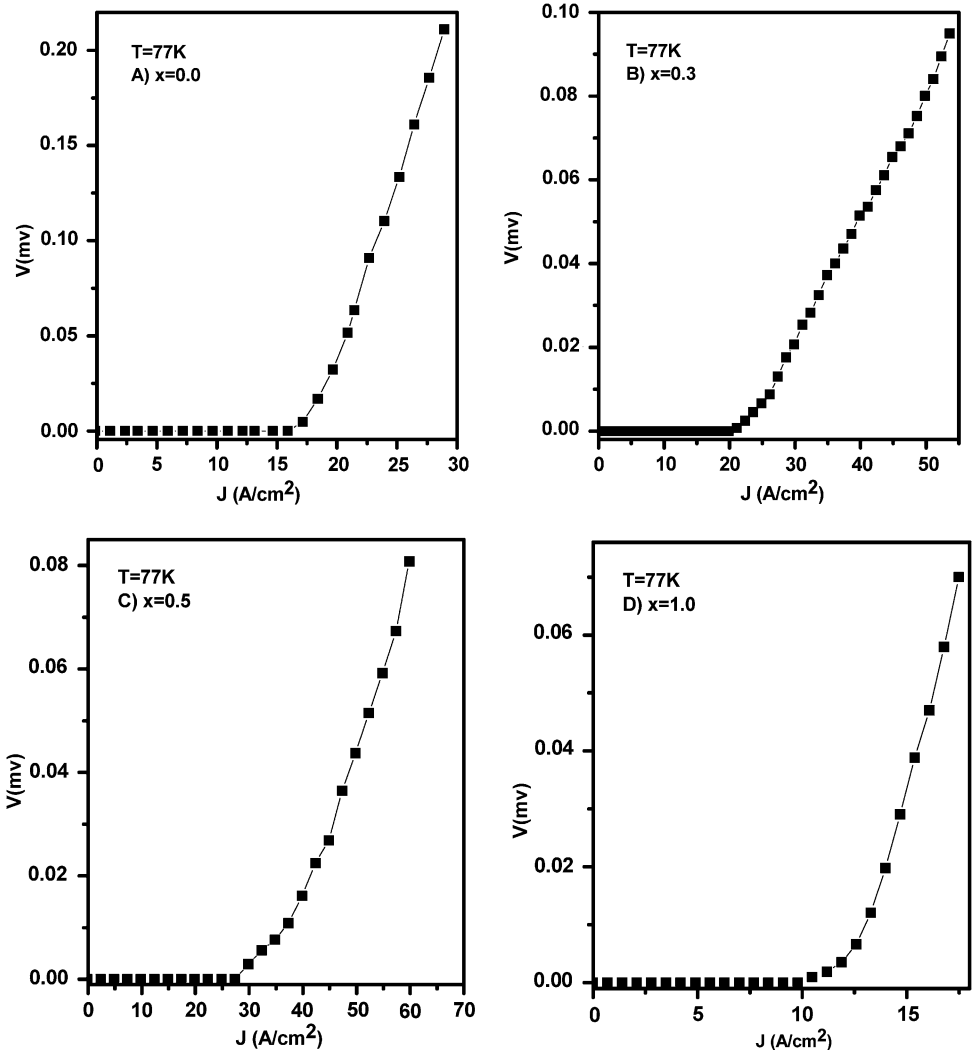
Fig. 9 Superconducting transition temperature versus hole concentration of Eu-free and -added samples: (**A**) $x = 0.0$, (**B**) $x = 0.3$, (**C**) $x = 0.5$, and (**D**) $x = 1.0$

Fig. 10 Critical current density of the $Bi_{1.6}Pb_{0.4}Sr_2Ca_2Cu_3$ $Oy + xEu_2O_3$ ($x = 0.0$–1.0) samples
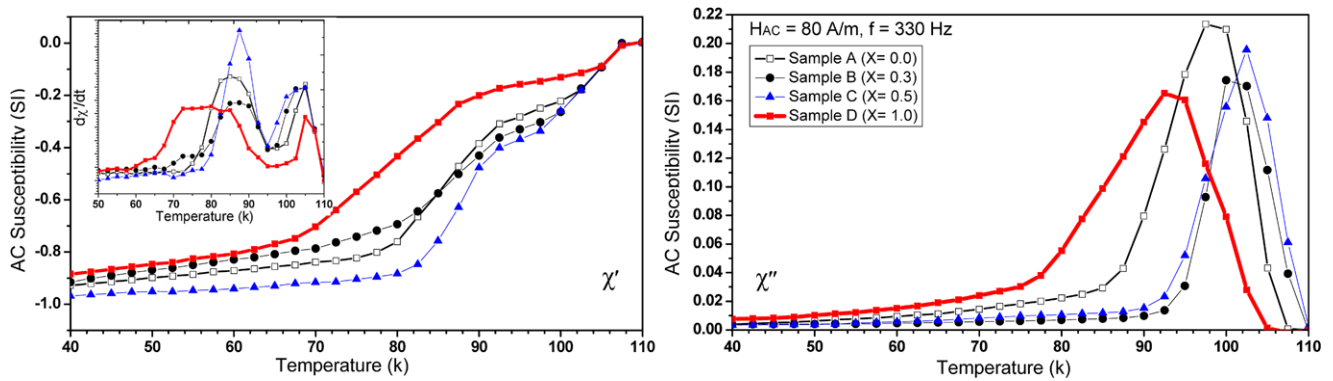
Fig. 11 AC magnetic susceptibility as a function of temperature for all samples (χ') Real part, (χ'') Imagery part. *Inset*: derivation of in-phase component versus temperature

peratures indicates gradual changes associated with the occurrence of bulk superconductivity, where superconducting current flows from grain to grain. The out-of-phase component, χ'', generally exhibits a peak with decreasing temperature below T_c, which is attributed to the absorption of magnetic energy of the superconductor from the AC field. Therefore, χ', is proportional to an amount of flux penetration into the body of the superconductor, while χ'' is associated with AC losses in the mixed state of superconductor [24].

In Fig. 11, the measurements of susceptibility versus temperature for Eu nanoparticles-free and Eu nanoparticles-added samples have been plotted for AC field of 80 A/m with $f = 330$ Hz. A broad magnetic transition for sample D ($x = 1.0$) is observed from measurement. Samples B ($x = 0.3$) and C ($x = 0.5$) have a slightly sharper transition compared to Eu-free sample. These results suggest that Eu nanoparticle-added samples up to $x = 0.5$ have a better intergranular coupling between the grains, which is in good agreement with DC electrical resistivity and J_c measurements. It is seen that the peak in χ'' shifts to higher temperature with increasing Eu nanoparticles concentration up to $x = 0.5$ while for sample D the peak shifts to lower temperatures. This means that AC losses for Eu nanoparticle-added samples (up to $x = 1.0$) start at higher temperatures compared with Eu-free sample. The curve obtained from derivation of the χ' versus temperature is inserted in Fig. 11, displaying intra- and inter-grain superconducting transition temperatures. The intra-grain transition temperature was determined to be about 105 K for all samples. However, the intergrain transition temperature shows an increase directly proportional to Eu nanoparticle concentration starting from 85 K for Eu-free sample and reaching 86.5 and 87.5 K for samples B and C, respectively. For sample D, the value is 78 K, indicating a drop in the increase of the intergrain transition temperature.

Figure 12 shows the AC susceptibility curves of the prepared bulk samples measured in the presence of the three magnetic field values. The diamagnetic onset temperature

of the superconducting transition is about 105 K for all samples. This temperature is independent of the applied field values for Eu nanoparticles-free and -added polycrystalline samples. It is well known that the minimum full flux penetration field, H_p, becomes larger by decreasing temperature from T_c to the temperature T_p, at which χ'' peaks occur. The value of the measured AC field at these temperatures is large enough to penetrate the center of the sample. When $H_{AC} = H_p$, the full flux penetration occurs. A function of the form $H_p = H_{AC}(1 - t)^n$ fits best the data obtained, where $t = (T/T_c)$ is the reduced temperature. The function obtained thereby is employed as a scaling function for temperature sweep measurements and it is most accurate at temperatures near T_c. By fitting H_{AC} versus $(1 - t)^n$ plot, we have found n for our samples. Figure 13 shows the temperature dependence of the intergranular critical current density, J_c, calculated from H_p values. According to Bean's model [24, 30], J_c at the peak temperature T_p can be calculated using the following relation:

$$J_c(T_p) = H_p/R \approx H_p/\sqrt{ab}$$

where $2a \times 2b$ is the cross section of the samples. It can be observed in Fig. 11 that there is the same behavior in increasing J_c for Eu nanoparticle-added samples as with the Eu-free sample. The result of the J_c measurements is in a good agreement with the result of J_c calculated from H_p values (enhanced intergrain coupling) thereby revealing the most important feature of this study. The enhancement observed in J_c suggests that poor amount of Eu nanoparticle addition can settle between grains and increase the connectivity of grains.

4 Conclusions

The samples with nominal composition $Bi_{1.6}Pb_{0.3}Sr_2$ $Ca_2Cu_3 + xEu_2O_3$ were prepared by the chemical sol–gel
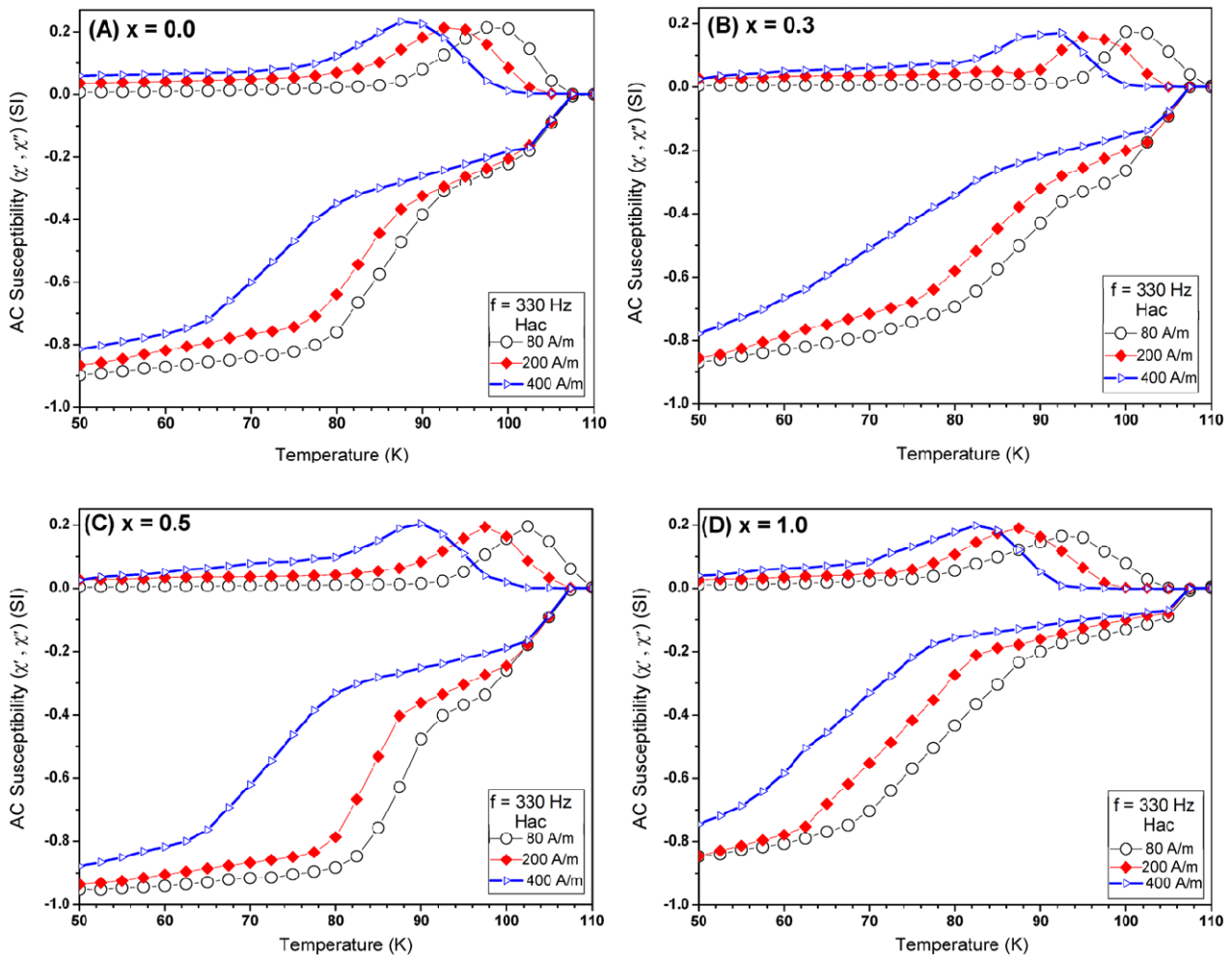
Fig. 12 AC magnetic susceptibility as a function of temperature for samples A, B, C and D
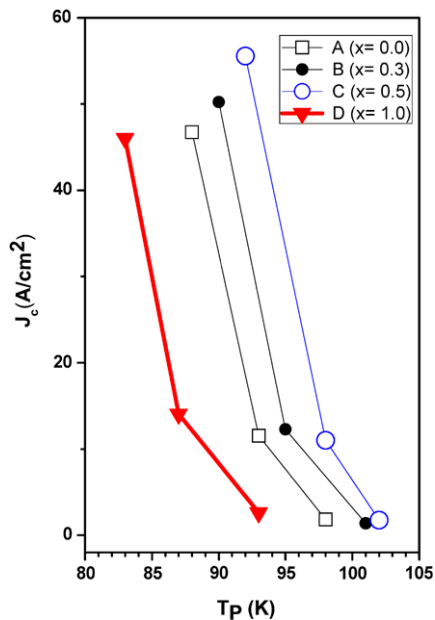

Fig. 13 Variation of critical current density with temperature

method. X-ray diffraction indicated that both Bi-2223 and Bi-2212 phases coexisted in the samples. The volume fraction which was estimated by XRD peaks intensities showed an increase in the volume fraction of the Bi-2223 high-T_c phase with increasing Eu nanoparticle concentration up to $x = 0.5$ wt%. SEM results showed that the added Eu nanoparticles settled among the grains boundaries. Based on electron diffraction results, the ratio of the lattice parameter b/a was estimated about 1.02, which is very close to the value obtained by the XRD results. EDX confirmed the presence of the desired elements in the chemical composition of the samples. $T_{c,\text{onset}}$ and $T_{c,R=0}$ of all the samples were obtained from DC electrical resistivity measurements. Hole concentration of the samples, calculated by the results of DC measurements, showed an increase with increasing Eu nanoparticle concentration up to $x = 0.5$ wt%. Critical current density measurement showed an enhancement in the J_c values with increasing Eu nanoparticle concentration up to $x = 0.5$ wt%. Intergranular coupling, intra- and inter-grain transition temperatures, and intergranular critical

current density were calculated by AC magnetic susceptibility measurements. Based on observation the Eu nanoparticle addition up to $x = 0.5$ wt% improves intergrain connectivity which results in better superconducting properties of BSCCO system. Critical current density is enhanced with Eu nanoparticle addition.

Conflict of interest The authors declare that they have no conflict of interest.

References

1. Maeda, H., Tnaka, Y., Fukutomi, M., Asano, T.: A new high-T_c oxide superconductor without a rare earth element. Jpn. J. Appl. Phys. **27**, 209–210 (1988)
2. Ozturk, O., Yegen, D., Yilmazlar, M., Varilci, A., Terzioglu, C.: The effect of cooling rates on properties of $Bi_{1.7}Pb_{0.35}$ $Sr_{1.9}Ca_{2.1}Cu_3O_y$ superconductors produced by solid-state reaction method. Phys., C Supercond. **451**, 113–117 (2007)
3. Michel, C., Hervieu, M., Borel, M.M., Grandin, A., Deslandes, F., Provost, J., Raveau, B.: Superconductivity in the Bi-Sr-Cu-O system. Z. Phys. B. **68**, 421–423 (1987)
4. Gul, I.H., Rehman, M.A., Ali, M., Maqsood, A.: Effect of vanadium and barium on the Bi-based (2223) superconductors. Physica C, Supercond. **432**, 71–80 (2005)
5. Lin, Z., Persson, M.: Crystallization and superconductivity of rapidly quenched (amorphous) Bi-Ca-Sr-Cu-O samples. Supercond. Sci. Technol. **1**, 198–200 (1988)
6. Xi, Z., Ji, C., Zhou, L.: 112–114 K superconductors $Bi_{1.8}Pb_{0.3}$ $Sr_2Ca_2Cu_3O_y$ by means of a three-step reaction process. Solid State Commun. **72**, 1015–1017 (1989)
7. Zhigadlo, N.D., Petrashko, V.V., Semenenko Yu, A., Panagopoulos, C., Cooper, J.R., Salje, E.K.H.: The effects of Cs doping, heat treatments on the phase formation and superconducting properties of (Bi, Pb)–Sr–Ca–Cu–O ceramics. Physica C, Supercond. **299**, 327–337 (1998)
8. Gul, I.H., Anis-ur-Rehman, M., Maqsood, A.: Temperature dependence of thermal and electrical conductivity of Bi-based high-T_c (2223) superconductor. Physica C, Supercond. **450**, 83–87 (2006)
9. Li, Y., Yang, B.: Doping of the Bi-Sr-Ca-Cu-O system with V_B elements and the effect on $Bi_2Sr_2Ca_2Cu_3O_y$ phase formation. J. Mater. Sci. Lett. **13**, 594–596 (1994)
10. Salamati, H., Kameli, P.: The effect of Bi-2212 phase on the weak link behavior of Bi-2223 superconductors. Physica C, Supercond. **403**, 60–66 (2004)
11. Halim, S.A., Khawaldeh, S.A., Mohamed, S.B., Azhan, H.: Superconducting properties of $Bi_{2-x}Pb_xSr_2Ca_2Cu_3O_y$ system derived via sol–gel and solid state routes. Mater. Chem. Phys. **61**, 251–259 (1999)
12. Dos Santos, C.A.M., Mochlecke, S., Kopelevich, Y., Machado, A.J.S.: Inhomogeneous superconducting in Bi_2Sr_2 $Ca_{1-x}Pr_xCu_2O_{8-z}$. Physica C, Supercond. **390**, 21–26 (2003)
13. Rentschler, T., Kemmler-Sack, S., Hartmann, M., Hubenen, R.P., Kesselar, P., Lichte, H.: Influence of Nd substitution on the superconducting properties of ceramics in the 2212 system $Bi_{2-w}Pb_wSr_{2-y}Nd_{x+y}Cu_xO_{8+z}$. Physica C, Supercond. **200**, 287–295 (1992)
14. Biju, A., Abhilash Kumar, R.G., Aloysius, R.P., Syamaprasad, U.: Structural and superconducting properties of $Bi_{1.7}Pb_{0.4}$ $Sr_{2-x}Gd_xCa_{1.1}Cu_2O_y$. Physica C, Supercond. **449**, 109–115 (2006)
15. Awana, V.P.S., Agarawal, S.K., Narlikar, A.V., Das, M.P.: Superconductivity in Pr- and Ce-doped $Bi_2CaSr_2Cu_2O_y$ system. Phys. Rev. B **48**, 1211–1216 (1993)
16. Berger, H., Ariosa, D., Gaal, R., Saleh, A., Margaritondo, G., Lee, S.F., Huang, S.H., Chang, H.W., Chuang, T.M., Liou, Y., Yao, Y.D., Hwu, Y.: Coexistance of ferromagnetism and high-temperature superconductivity in Dy-doped BiPbSrCaCuO. Surf. Rev. Lett. **9**, 1109–1112 (2002)
17. Zelati, A., Amirabadizadeh, A., Kompany, A., Salamati, H., Sonier, J.E.: Manufacture and characterization of Dy_2O_3 nanoparticles via X-ray diffraction, TEM and PL. Indian J. Inf. Sci. Technol. **6**(12), 5552–5558 (2013)
18. Nabil, A., Yahya, A., Abd-Shukor, R.: Effect of different nano-sized MgO on the transport critical current density of $Bi_{1.6}Pb_{0.4}Sr_2Ca_2Cu_3O_{10}$ superconductor. J. Supercond. Nov. Magn. (2013). doi:10.1007/s10948-013-2302-5
19. Mawassi, R., Marhaba, S., Roumié, M., Awad, R., Korek, M., Hassan, I.: Improvement of superconducting parameters of $Bi_{1.8}Pb_{0.4}Sr_2Ca_2Cu_3O_{10+\delta}$ added with nano-Ag. J. Supercond. Nov. Magn. (2013). doi:10.1007/s10948-013-2408-9
20. Kong, W., Abd-Shukor, R.: Enhanced electrical transport properties of nano $NiFe_2O_4$ added $(Bi_{1.6}Pb_{0.4})Sr_2Ca_2Cu_3O_{10}$ superconductor. J. Supercond. Nov. Magn. **23**, 257–263 (2010)
21. Agail, A., Abd-Shukor, R.: Transport current density of $(Bi_{1.6}Pb_{0.4})Sr_2Ca_2Cu_3O_{10}$ superconductor added with different nano-sized ZnO. Appl. Phys. A **112**, 501–506 (2013)
22. Mao, C., Zhou, L., Wu, X., Sun, X.: The combination of the polymeric solution sol–gel process and combustion synthesis to manufacture BiPbSrCaCuO powder. Supercond. Sci. Technol. **9**, 994–1000 (1996)
23. Tampieri, A., Celotti, G., Lesca, S., Bezzi, G., La Torretta, T.M.G., Magnani, G.: Bi(Pb)-Sr-Ca-Cu-O (2223) superconductor prepared by improved sol–gel technique. J. Eur. Ceram. Soc. **20**, 119–126 (2000)
24. Ghazanfaria, N., Kilic, A., Gencerb, A., Ozkana, H.: Effects of Nb_2O_5 addition on superconducting properties of BSCCO. Solid State Commun. **144**, 210–214 (2007)
25. Saleh, S.A.: Studies on sintering effect on the structural and transport properties of (2223) phase. Physica C, Supercond. **444**, 40–44 (2006)
26. Mia, S., Balanetskyya, S., Grushkoa, B.: A study of the Al-rich part of the Al-Ru alloy system. Intermetallics **11**, 643–649 (2003)
27. He, H.P., Huang, X.J., Chen, L.Q.: An effective way to detect the secondary phase in Sr-doped $LaInO_3$. J. Phys. Chem. Solids **62**, 701–709 (2001)
28. Kocabas, K., Ciftcioglu, M.: The effect of Sb substitution of Cu in $Bi_{1.7}Pb_{0.3}Sr_2Ca_2Cu_{3-x}Sb_xO_y$ superconductors. Phys. Status Solidi A **177**, 539–545 (2000)
29. Bilgili, O., Selamet, Y., Kocabas, K.: Effects of Li substitution in Bi-2223 superconductors. J. Supercond. Nov. Magn. **21**, 439–449 (2008)
30. Bean, C.P.: Magnetization of high-field superconductors. Rev. Mod. Phys. **36**, 31–39 (1964)